

# Impulsive X-ray Raman excitation of NO<sub>2</sub>

Daniel J. Haxton<sup>1</sup>

<sup>1</sup>*Department of Physics, University of California, Berkeley CA 94720*

We investigate impulsive X-ray Raman excitation of the NO<sub>2</sub> molecule. We seek to optimize population transfer to valence states of the NO<sub>2</sub> molecule using using 1fs pulses tuned below the Oxygen K-edge, and detect subsequent coherent electron motion among valence excited states by using a second, weak X-ray pulse with variable time delay that ionizes a Nitrogen 1s electron. Toward these ends, impulsive X-ray Raman excitations were calculated in the fixed-nuclei approximation using the multiconfiguration time-dependent Hartree-Fock (MCTDHF) method. Fixing the duration but varying the central frequency and intensity of the pulse, not considering chirp, we find optimum population transfer at intensity approximately  $3 \times 10^{17}$  W cm<sup>-2</sup>, an intensity for which 2nd order perturbation theory is no longer applicable, with the central frequency substantially 8eV red-detuned from the 2nd order optimum.

PACS numbers: 33.20.Fb 33.20.Rm 42.65.Re 42.65.Dr

## I. INTRODUCTION

The Multiconfiguration time-dependent Hartree-Fock (MCTDHF) method is capable of calculating arbitrary nonperturbative quantum dynamics of electrons in medium-sized molecules. We have applied our implementation of it [1–4] to predict valence population transfer due to stimulated X-ray transitions in the NO<sub>2</sub> molecule, in the fixed-nuclei approximation.

It has been assumed that transitions via discrete states are most effective in driving this process [5, 6]. A calculation has demonstrated [5] that impulsive X-ray Raman would drive significant population transfer at second order in the field intensity.

However, in the present study of the NO<sub>2</sub> molecule, we find that these two assumptions fail. For the NO<sub>2</sub> molecule, we demonstrate that population transfer via the continuum is a dominant mechanism for attosecond X-ray Raman transitions, and that the behavior at optimum intensity is much different from the 2nd order result.

## II. MCTDHF CALCULATION OF NO<sub>2</sub>

Our implementation of MCTDHF for electrons in molecules has already been described [1–3] and our code is available [4]. Briefly, the MCTDHF method solves the time-dependent Schrodinger equation using a time-dependent linear combination of Slater determinants, with time-dependent orbitals in the Slater determinants. The nonlinear working equations are obtained through application of the Lagrangian variational principle [7, 8] to this wave function ansatz.

The representation of orbitals using sinc basis functions is described in Ref. [3]. For NO<sub>2</sub>, we use a grid of  $55 \times 55 \times 55$  (=166375) product sinc basis functions for the orbitals. The spacing between the functions is 0.2975614 bohr (about 0.56 Angstrom). Complex scaling and stretching is applied starting at  $\pm 4$  bohr in the  $x$ ,  $y$ , and  $z$  directions.

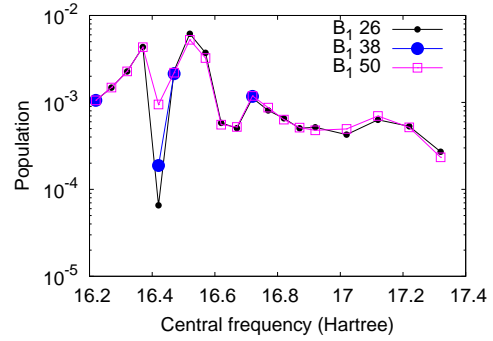


FIG. 1. (Color online) Convergence of the  $B_1$  population at  $10^{17}$  W cm<sup>-2</sup>, with respect to the order of the Lebedev quadrature used for the orientation average of fixed-nuclei calculations.

The calculations are performed with full configuration interaction, 23 electrons in 15 orbitals, giving 621075 Slater determinants which are contracted to 305760 spin-adapted linear combinations and distributed among processors. The mean field time step was 0.02 atomic time units (approximately one half attosecond).

We calculate population transfer for the valence  $B_1$ ,  $B_2$ , and  $A_2$  states. We integrate the result over orientations using Lebedev quadrature. Comparing 38- and 50-point quadrature, we find that most of the results are converged with 38-point quadrature. We have not attempted to demonstrate the convergence of these results beyond 50-point quadrature due to computer resources. In Figure 1 we show the convergence of the  $B_1$  population at  $10^{17}$  W cm<sup>-2</sup>, with respect to the order of the Lebedev quadrature.

Due to symmetry, and within the rotating wave approximation, only seven of the 50 points need to be calculated. Each central frequency and intensity required approximately 10,000 cpu-hours to calculate: seven calculations, 121 processors each, and about twelve hours per calculation.

The energies of the valence states are shown in Table I.

	Ref. [10]	Present
B <sub>1</sub>	2.827 eV	4.294 eV
B <sub>2</sub>	3.239 eV	3.850 eV
A <sub>2</sub>	3.977 eV	4.009 eV

TABLE I. Transition energies for valence states: vertical transition energies previously calculated from Ref. [10], and transition energies for states used to define populations from the MCTDHF calculation.

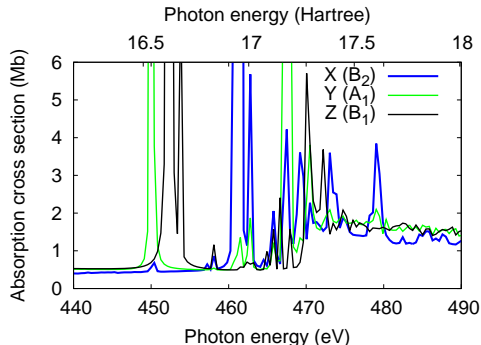


FIG. 2. (Color online) NO<sub>2</sub> photoionization cross section calculated in the vicinity of the Oxygen K-edge using a 10fs MCTDHF calculation with a weak pulse. The K-edge is artificially low in these calculations.

We provide vertical transition energies from the literature, and also report our transition energies. These are the transition energies of the states used for projection, relative to the initial state used in the MCTDHF propagation. The states are not used in the MCTDHF calculation, and we have demonstrated [9] that these transition energies do not correspond with transition energies apparent from MCTDHF calculations. They are nevertheless included here for the sake of completeness.

Due to the spacing of sinc functions – again, 0.2975614 bohr – and the fact that we have not elaborated our method with any pseudopotential or effective theory to account for the truncation in momentum space, the core transitions that drive the X-ray Raman process are shifted substantially downward in energy. As can be seen in Fig. 2, the Oxygen K-edge appears at approximately 470eV in these calculations, not the actual 540eV.

Fig. 2 shows the photoionization cross section calculated in the neighborhood of the Oxygen K-edge. The magnitude of the cross section above and below the edge (about 0.5 and a bit more than 1.0 respectively) agree well with figure 5.10 in Berkowitz’s compilation [11]. The three peaks at about 450 (A<sub>1</sub>), and 452 & 453 (B<sub>1</sub>) correspond to excitations to 6a<sub>1</sub> and 2b<sub>1</sub> from the Oxygen 1s σ<sub>g</sub> orbital, and correspond with the peaks observed at approximately 530, 532, and 533 in experiment [12–14]. Relative to these peaks, there is also a pair of B<sub>2</sub> states, at about 462eV, both spin couplings for excitation to 5b<sub>2</sub>, and the K-edge lies at about 468eV. It is

clear that the K-edge is too high in energy, and the B<sub>2</sub> states are too low, because the B<sub>2</sub> states are observed as a broad core-excited shape resonance in experiment. Experiment [12–14] gives a A<sub>1</sub> to B<sub>2</sub> excitation energy of 15eV, and a K-edge about 12eV above A<sub>1</sub>; here they are found at about 12 and 18eV, respectively.

### III. RESULTS FOR IMPULSIVE X-RAY RAMAN EXCITATION OF NO<sub>2</sub>

The results for population transfer using 1fs linearly polarized pulses are shown in Figure 3.

The best population transfer is obtained for the B<sub>1</sub> state, at approximately  $3 \times 10^{17}$  W cm<sup>-2</sup>, substantially red-detuned from the second-order optimum. However the optimum population transfer is only 1% with these one-femtosecond, linearly polarized pulses. We will vary chirp and duration in future work.

The second-order behavior is visible in Fig. 3 in the bold black line with open squares, corresponding to intensity  $1 \times 10^{15}$  W cm<sup>-2</sup>. This result has been multiplied by 100 in the figure, and lies on top of the orange (grey) line with solid squares in the figure, the line corresponding to intensity  $1 \times 10^{16}$  W cm<sup>-2</sup>, on the left-hand side of the figure at lower central frequency. Thus, one can see that even at  $1 \times 10^{16}$  W cm<sup>-2</sup>, when the central frequency is low such that the pulse is not resonant with any of the near-edge fine structure nor the continuum above the edge, the behavior is still second-order.

However, as the intensity is increased, strong nonlinear effects arise that are contrary to the conventional wisdom. We see here that the optimum population transfer is obtained with central frequency much different from the the second-order optimum. In Fig. 3, we see that as the intensity is increased, a strong minimum in the population transfer for the B<sub>1</sub> and A<sub>2</sub> states develops around 447eV in these calculations. This minimum persists for a range of intensities. Among the calculations we have performed, the overall optimum population transfer is seen to occur to the B<sub>1</sub> state, below this robust minimum, at  $3.16 \times 10^{17}$  W cm<sup>-2</sup>, and a central frequency of 444eV in these calculations. 444eV is approximately 6eV below the lowest state responsible for the near-edge fine structure, the A<sub>1</sub> excitation  $1s \rightarrow 6a_1$ , and 8eV below the 2nd order optimum.

We plan further calculations and modeling to interrogate the nature of this excitation. However, it seems clear from the results that this excitation is driven by nonresonant Raman via the  $1s^{-1}$  continuum. For each of the three states, the excitation probability drops steeply as the central frequency is decreased on the left side of the figures. This behavior is what we would expect from nonresonant Raman via the Oxygen  $1s^{-1}$  continuum at higher energy. In contrast, if population transfer were occurring via direct, one-electron Raman, or via the continuum excitations of the 2s or 2p electron(s) or the 1s electrons of Nitrogen, we would expect relatively constant

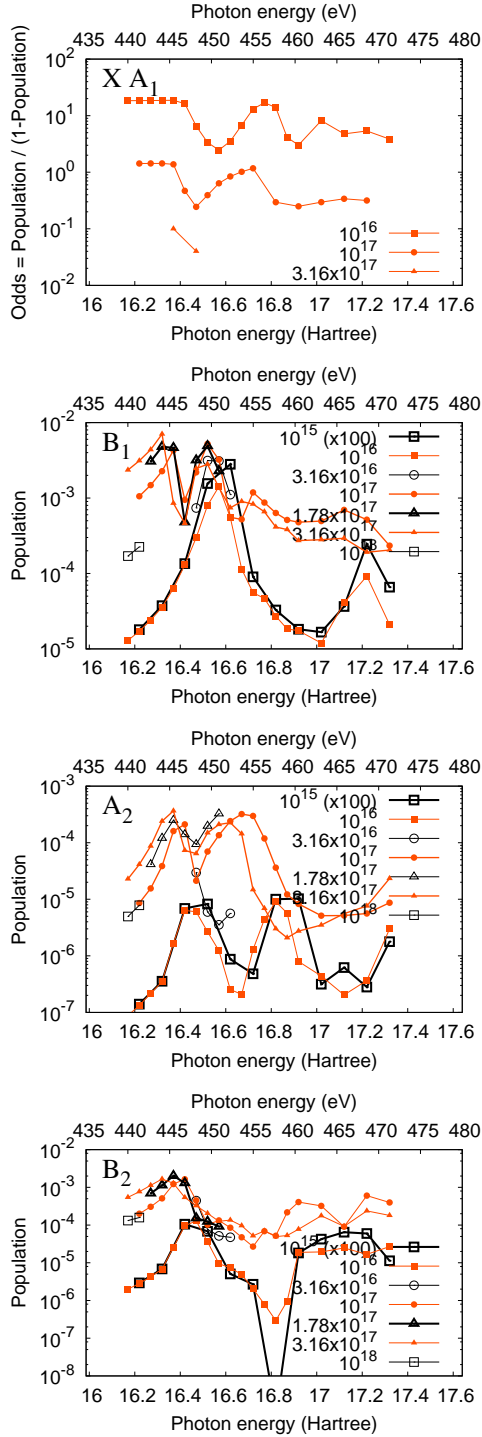


FIG. 3. (Color online) Results for population transfer to the  $B_1$ ,  $A_2$ , and  $B_2$  valence excited states of  $\text{NO}_2$ , and odds for remaining in the ground state, averaged over orientation, for 1fs pulses, as labeled. Different intensities are plotted with different lines and labeled in Watts per square centimeter.

behavior on the left side of the figure.

#### IV. CONCLUSION

We have demonstrated that optimum population transfer to valence electronic states in  $\text{NO}_2$  by linearly polarized 1fs pulses tuned to the Oxygen K-edge occurs 8eV red-detuned from the 2nd order optimum and 6eV red-detuned from any near-edge fine structure, at approximately  $3 \times 10^{17} \text{ W cm}^{-2}$ . It appears to proceed via nonresonant Raman via the K-edge continuum. These results refute commonly-held assumptions about the nature of impulsive Raman transitions in molecules: the optimum population transfer occurs at an intensity such that 2nd order perturbation theory is no longer applicable, and population transfer occurs at a central frequency that is far red-detuned from the optimum at 2nd order. In future work, we will more closely examine the mechanisms behind the optimum population transfer via impulsive X-ray Raman transitions in  $\text{NO}_2$ .

[1] D. J. Haxton, K. V. Lawler, and C. W. McCurdy, Phys. Rev. A **83**, 063416 (2011).

[2] D. J. Haxton and C. W. McCurdy, Phys. Rev. A **91**, 012509 (2015).

- [3] J. R. Jones, F.-H. Rouet, K. V. Lawler, E. Vecharynski, K. Z. Ibrahim, S. Williams, B. Abeln, C. Yang, D. J. Haxton, C. W. McCurdy, X. S. Li, and T. N. Rescigno, Published online in Molecular Physics April 27, 2016.
- [4] D. J. Haxton, C. W. McCurdy, T. N. Rescigno, K. V. Lawler, J. Jones, B. Abeln, and X. Li, LBNL-AMO-MCTDHF.
- [5] S. Miyabe and P. Bucksbaum, Phys. Rev. Lett. **114**, 143005 (2015).
- [6] S. Mukamel, D. Healion, Y. Zhang, and J. D. Biggs, Ann. Rev. Phys. Chem **64**, 101 (2013).
- [7] J. Broeckhove, L. Lathouwers, E. Kesteloot, and P. V. Leuven, Chem. Phys. Lett. **149**, 547 (1988).
- [8] K. Ohta, Phys. Rev. A **70**, 022503 (2004).
- [9] D. J. Haxton, K. V. Lawler, and C. W. McCurdy, Phys. Rev. A **86**, 013406 (2012).
- [10] N. Wu and X. Chen, The Journal of Physical Chemistry A **116**, 6894 (2012).
- [11] J. Berkowitz, in *Atomic and Molecular Photoabsorption*, edited by J. Berkowitz (Academic Press, London, 2002) pp. 237 – 316.
- [12] A. Jurgensen and R. G. Cavell, Chemical Physics **257**, 123 (2000).
- [13] T. Gejo, Y. Takata, T. Hatsui, M. Nagasono, H. Oji, N. Kosugi, and E. Shigemasa, Chemical Physics **289**, 15 (2003), decay Processes in Core-excited Species.
- [14] M. Piancastelli, V. Carravetta, I. Hjelte, A. D. Fanis, K. Okada, N. Saito, M. Kitajima, H. Tanaka, and K. Ueda, Chemical Physics Letters **399**, 426 (2004).

